Interplanetary Type III Bursts and Electron Density Fluctuations in the Solar Wind

V. Krupar[1,2,3] , M. Maksimovic[4], E. P. Kontar[5] , A. Zaslavsky[4], O. Santolik[3,6] , J. Soucek[3] , O. Kruparova[3],
J. P. Eastwood[7] , and A. Szabo[2]

[1] Universities Space Research Association, Columbia, MD, USA; vratislav.krupar@nasa.gov
[2] NASA Goddard Space Flight Center, Greenbelt, MD, USA; adam.szabo-1@nasa.gov
[3] Institute of Atmospheric Physics CAS, Prague, Czech Republic; soucek@ufa.cas.cz, ok@ufa.cas.cz
[4] LESIA, UMR CNRS 8109, Observatoire de Paris, Meudon, France; milan.maksimovic@obspm.fr, arnaud.zaslavsky@obspm.fr
[5] School of Physics and Astronomy, University of Glasgow, Glasgow, G12 8QQ, UK; eduard.kontar@glasgow.ac.uk
[6] Faculty of Mathematics and Physics, Charles University, Prague, Czech Republic; os@ufa.cas.cz
[7] The Blackett Laboratory, Imperial College London, London, UK; jonathan.eastwood@imperial.ac.uk
Received 2017 December 1; revised 2018 March 9; accepted 2018 March 9; published 2018 April 17

Abstract

Type III bursts are generated by fast electron beams originated from magnetic reconnection sites of solar flares. As propagation of radio waves in the interplanetary medium is strongly affected by random electron density fluctuations, type III bursts provide us with a unique diagnostic tool for solar wind remote plasma measurements. Here, we performed a statistical survey of 152 simple and isolated type III bursts observed by the twin-spacecraft *Solar TErrestrial RElations Observatory* mission. We investigated their time–frequency profiles in order to retrieve decay times as a function of frequency. Next, we performed Monte Carlo simulations to study the role of scattering due to random electron density fluctuations on time–frequency profiles of radio emissions generated in the interplanetary medium. For simplification, we assumed the presence of isotropic electron density fluctuations described by a power law with the Kolmogorov spectral index. Decay times obtained from observations and simulations were compared. We found that the characteristic exponential decay profile of type III bursts can be explained by the scattering of the fundamental component between the source and the observer despite restrictive assumptions included in the Monte Carlo simulation algorithm. Our results suggest that relative electron density fluctuations $\langle \delta n_e \rangle / n_e$ in the solar wind are 0.06–0.07 over wide range of heliospheric distances.

Key words: scattering – Sun: radio radiation – solar wind

1. Introduction

Solar flares are associated with intense radio signals in a wide range of frequencies, in particular with fast-drifting type III bursts (Bastian et al. 1998; Miteva et al. 2017). They are produced by beams of suprathermal electrons accelerated at reconnection sites of solar flares traveling outward along open magnetic filed lines through the corona and the interplanetary medium (Wild 1950). Along their path, these beams interact with the ambient medium generating radio emissions at the electron plasma frequency f_{pe} (the fundamental component) and/or at its first harmonic $2f_{pe}$ (the harmonic component) via the plasma emission mechanism (Ginzburg & Zheleszniakov 1958; Cairns & Robinson 1995; Ergun et al. 1998). Both components are often simultaneously observed at decametric and shorter wavelengths (i.e., those generated in the corona) when the harmonic component simultaneously occurs roughly at twice the frequency of the fundamental one (Stewart 1974). Typically, the fundamental component is more intense and has a higher degree of circular polarization when compared to the harmonic one (Dulk & Suzuki 1980). For type III bursts originating from the interplanetary space—which are within the scope of this study—it is nearly impossible to separate the two components in time and frequency or by polarization measurements (Reiner et al. 1998; Gopalswamy et al. 2005; Krupar et al. 2015). However, Kellogg (1980) developed a timing method to identify the particular component of interplanetary type III bursts for rare cases when electron beams are observed in situ at spacecraft. For such type III bursts, the initial radiation is almost always the fundamental component, while in the late phases, it may be one or the other (Dulk et al. 1998). The duration of interplanetary type III bursts ranges from minutes to hours, and an exponential decay of the radio flux density is frequently observed (Alvarez & Haddock 1973; Evans et al. 1973).

Type III bursts are simultaneously measured over a broad range of angles, even if their sources are located behind the Sun (Bonnin et al. 2008). Their sources lie at considerably larger radial distances than average electron density models predict within a factor of five and three for the fundamental and harmonic components, respectively (Reiner et al. 2009; Martínez Oliveros et al. 2012). Moreover, observed source sizes of interplanetary type III bursts are apparently so extended that they sometimes spread over the entire inner heliosphere (Krupar et al. 2014a). These features are often attributed to scattering of radio beams by electron density inhomogeneities as they propagate from the source to the spacecraft (Steinberg et al. 1984, 1985; Bastian 1994, 1995). The effects of scattering were recently also observed at decameter wavelength using fine structures in coronal type III bursts (Kontar et al. 2017). The role of refraction and scattering of interplanetary radio emissions can be studied using a geometric optics method and Monte Carlo simulations (Hollweg 1968; Melrose 1980; Thejappa et al. 2007; Thejappa & MacDowall 2008).

Here, we examine radio measurements obtained by the twin-spacecraft *Solar TErrestrial RElations Observatory* (STEREO) mission with a circumsolar orbit around ∼1 astronomical unit
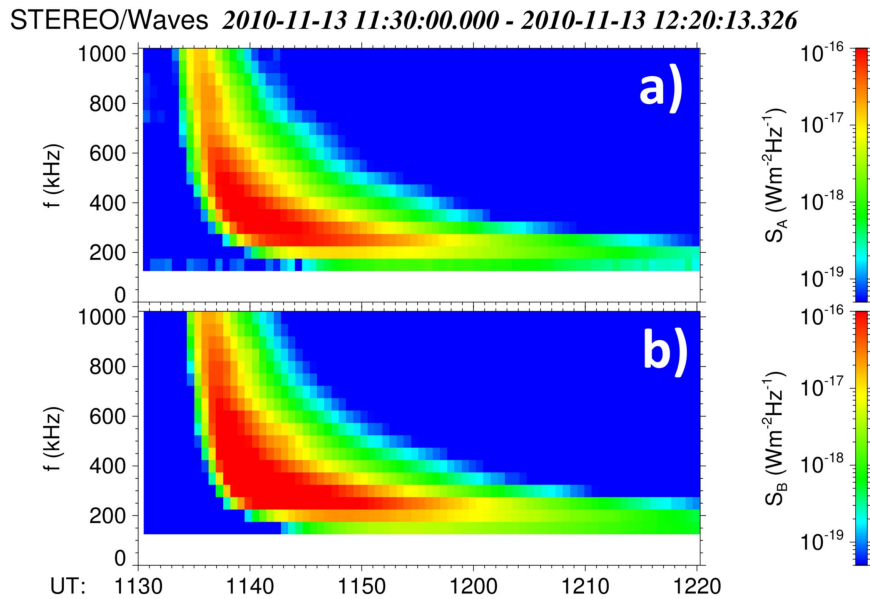
Figure 1. Radio measurements of the 2010 November 13 type III burst. (a), (b) Radio flux density S for *STEREO-A* and *STEREO-B*.

(1 au = 149,598,000 km). Both spacecraft carry the *STEREO/ Waves/High Frequency Receiver* (125 kHz–16 MHz) that provides us with comprehensive measurements of the electric field fluctuations using three monopole antennas (Bale et al. 2008; Bougeret et al. 2008). We analyze radio observations of type III bursts recorded between 125 and 975 kHz (17 frequency channels with a bandwidth of 50 kHz). Higher frequencies have been excluded from this study due to insufficient time resolution of the *STEREO*/Waves instrument, which is 38 s. Effective antenna parameters have been retrieved using observations of galactic background and auroral kilometric radiation (Zaslavsky et al. 2011; Krupar et al. 2012). The time profiles of the bursts are also simulated using radio-wave propagation in the heliosphere, with density fluctuations allowing us to infer density fluctuations that are consistent with the observations.

In this paper, we present a statistical survey of type III burst decay times that can be used to estimate relative electron density fluctuations in the solar wind. In Section 2, we present our analysis of *STEREO*/Waves measurements (Section 2.1) and its comparison to results of Monte Carlo simulations (Section 2.2). The discussion and summary are presented in Section 3.

2. Observation and Analysis

2.1. STEREO/Waves Measurements

We performed a statistical analysis of 152 type III radio bursts observed by *STEREO* between 2007 May and 2013 February. The separation angle between the spacecraft in the ecliptic plane ranged between 7° (2007 May) and 180° (2011 February). Only intense, simple, and isolated cases have been included. This data set has already been used to study radio source locations and radio flux variations with frequency from Krupar et al. (2014a, 2014b). As an example from our list of events, we show an analysis of a type III burst from 2010 November 13 that has been linked to a C1.3 solar flare located at S23°W16°. Figure 1 shows the flux density S from *STEREO-A* and *STEREO-B*. Both spacecraft detected a simple and isolated type III burst with an onset time at about 11:35 UT.

During this event, *STEREO-A* was at 84° west from a Sun–Earth line at 0.97 au from the Sun, whereas *STEREO-B* was at 83° east and 1.08 au from the Sun.

Figure 2 displays fixed-frequency light curves of the same event in four frequency channels (125, 375, 675, and 975 kHz). The exponential decay of the flux density S over several decades can be clearly seen. Through further analysis, we calculated median values of the flux density S for each frequency channel separately to identify background level (red lines in Figure 2). We use only data points above this threshold. We analyze data points between the peak time (t_{peak}) and the last value above this level (i.e., between dashed blue lines in Figure 2). We assume an exponential decay profile of the flux density S, which can be described by the following equation:

$$S(t) = \frac{I}{\tau} \exp\left(\frac{t_{\mathrm{peak}} - t}{\tau}\right), \qquad (1)$$

where t is the time and t_{peak} corresponds to the time of the peak flux density. Coefficients I and τ are parameters of a gradient-expansion algorithm to compute a nonlinear least-squares fit. Figure 2 shows the results of this fitting for decay flux density profiles in green. As expected, the calculated decay times τ increase with decreasing frequency f. Results from both spacecraft are about the same.

We performed the above-described analysis of the exponential decay times τ on 152 type III bursts case by case. Although our data set spans periods of solar minimum to near solar maximum, we do not observe any significant variations of τ in time. Figure 3 displays histograms of the decay times τ for four frequency channels (125, 375, 675, and 975 kHz). As expected, τ increases with decreasing frequency. We note that only 35% (*STEREO-A*) and 25% (*STEREO-B*) of events were measured down to 125 kHz (Krupar et al. 2014b). This low-frequency cut-off can be explained as an intrinsic characteristic of the radiation mechanism, an effect of the directivity of the radiation, and propagation effects between the source and the observer (Leblanc et al. 1995). For the statistical analysis, we use median values due to the log-normal character of the τ distributions. Figure 4 shows median values of decay times τ as
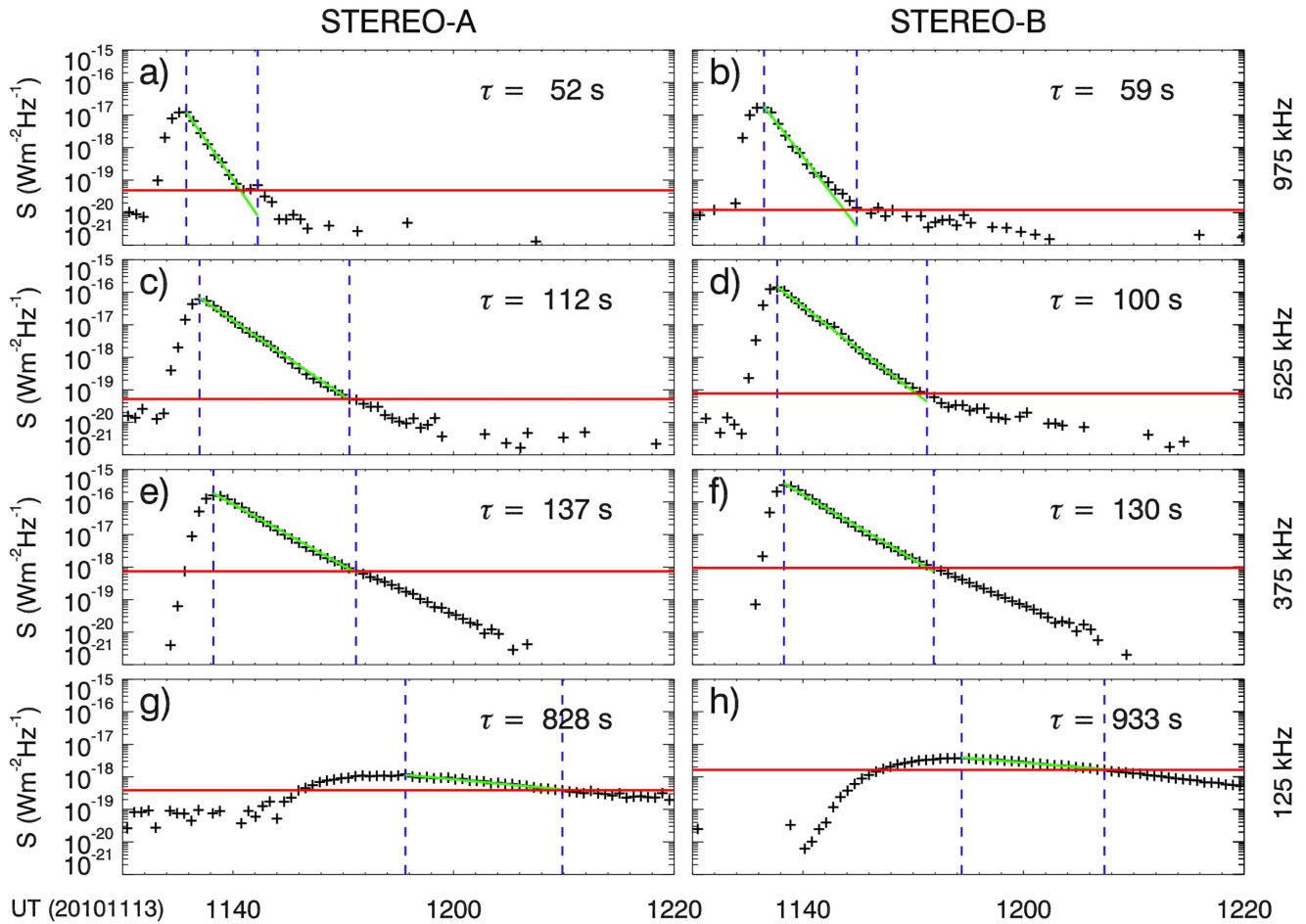
Figure 2. Radio measurements of the 2010 November 13 type III burst. (a)–(h) Fixed-frequency light curves of the radio flux density recorded by *STEREO-A* and *STEREO-B* for four frequency channels. The red lines show median values in the given time intervals. The dashed lines denote peak fluxes and last points above the median values. The green lines show the results of decay time fitting (Equation (1)).

a function of frequency. We assume that the decay times τ are statistically frequency depend as

$$\tau(f) = \alpha f^\beta. \tag{2}$$

This model fit the data very well for both spacecraft. We obtained spectral indices β of -1.18 ± 0.2 and -1.25 ± 0.2 for *STEREO-A* and *STEREO-B*, respectively. These values were calculated by minimizing the χ^2 error statistic with the 1σ uncertainty estimates. A similar study of 79 type III bursts observed by the *OGO*-5 spacecraft was performed by Alvarez & Haddock (1973). They analyzed nine frequency channels between 50 kHz and 3.5 MHz, obtaining a spectral index β of -0.95. Evans et al. (1973) investigated 35 type III bursts observed by the RAE-1 and IMP-6 spacecraft between 67 kHz and 2.8 MHz. They obtained a spectral index β of -1.08, which is close to our findings.

2.2. Monte Carlo Simulations

Thejappa et al. (2007) developed a Monte Carlo simulation code to quantify effects of refraction and scattering on propagation of radio emissions generated at $f = 120$ kHz, when observed at 1 au. For this purpose, they employed a set of six first-order differential equations derived by Haselgrove (1963) to retrieve the position and direction vectors $\boldsymbol{R}$ and $\boldsymbol{T}$, respectively. They launched 1000 randomly directed rays from

the isotropic point source located at altitudes with plasma levels corresponding to 115 kHz (the fundamental component; $f = 1.05 f_{\text{pe}}$) and 60 kHz (the harmonic component; $f = 2 f_{\text{pe}}$). For the refraction, the spherically symmetric solar wind electron density model of Bougeret et al. (1984) was employed ($n \sim r^{-2.10}$). For the scattering, Thejappa et al. (2007) assumed the power spectrum of electron density fluctuations in the solar wind P_n in the inertial range to be proportional to the spatial wavenumber q as $P_n(q) \sim q^{-11/3}$ (i.e., the Kolmogorov spectrum). They used an empirical formula for the outer scale of the electron density fluctuations l_o by Wohlmuth et al. (2001), while the inner scale l_i was assumed to be 100 km (Manoharan et al. 1987; Coles & Harmon 1989). The relative electron density fluctuations $\epsilon = \langle \delta n_e \rangle / n_e$ was set to be 0.07, which corresponds to results by Bavassano & Bruno (1995). They investigated 4693 intervals with a length of 45 minutes recorded by the two *Helios* spacecraft covering heliospheric distances between 0.3 au and 1 au to retrieve the relative density fluctuations ϵ. Bavassano & Bruno (1995) concluded that in about 86% of cases, ϵ has a value below 0.1. The scattering is included by adding a perturbation vector $\langle \boldsymbol{q} \rangle$ to $\boldsymbol{T}$ after each step when a ray suffers a regular refraction in a layer of thickness ΔS corresponding to the ray path length. Thejappa et al. (2007) used $\Delta S = 10l$ in the simulation code, where l is the effective scale of electron density fluctuations defined as $l = l_i^{1/3} l_o^{2/3}$. The vector $\langle \boldsymbol{q} \rangle$ is calculated from a Gaussian
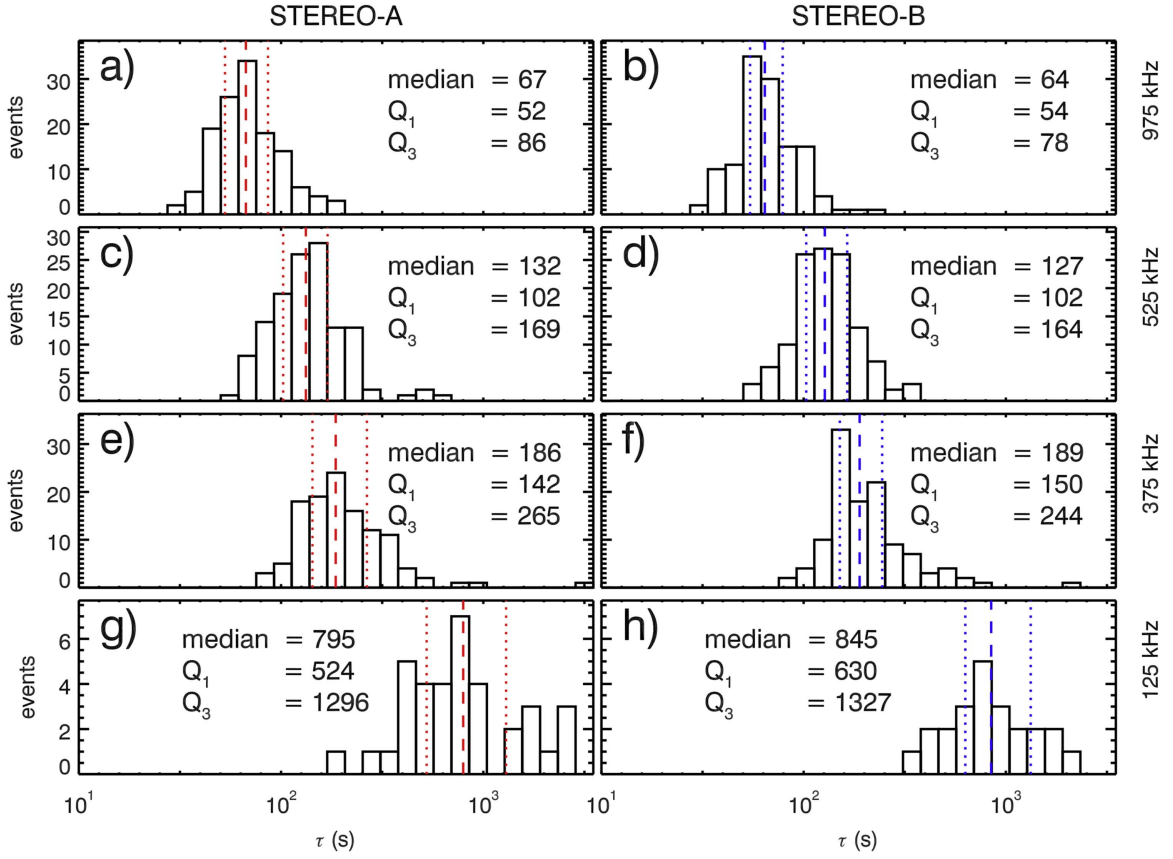
Figure 3. Results of the statistical survey of 152 type III radio bursts. (a)–(h) Histograms of decay times τ for *STEREO-A* and *STEREO-B*.
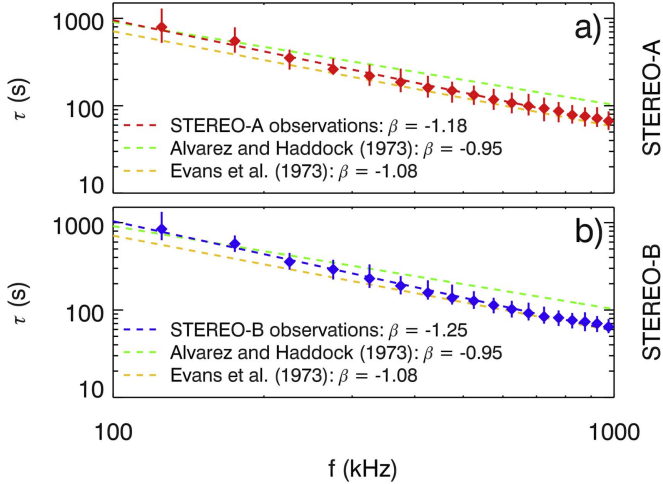
Figure 4. Results of the statistical survey of 152 type III radio bursts. (a), (b) Median values of τ for *STEREO-A* and *STEREO-B* as a function of frequency. Error bars are the 25th/75th percentiles. The red and blue dashed lines represent the results of power-law fitting (Equation (2)) for *STEREO-A* and *STEREO-B*, respectively. The green and yellow dashed lines correspond to results of Alvarez & Haddock (1973) and Evans et al. (1973), respectively.

distribution of random numbers with a zero mean and a standard deviation of

$$\sigma = \sqrt{\frac{\pi \Delta S}{l}} \left(\frac{f_{\mathrm{pe}}}{f}\right)^2 \frac{\epsilon}{\sqrt{1 - (f_{\mathrm{pe}}/f)^2}}. \qquad (3)$$

These rays are traced until they cross the sphere of 1 au radius (i.e., $|\mathbf{R}| = 1$ au). Thejappa et al. (2007) concluded that

scattering by random electron density fluctuations may extend the angular range of visibilities of the fundamental and harmonic emissions from 18° to 100°, and from 80° to 150°, respectively.

We have implemented the Monte Carlo technique of Thejappa et al. (2007) to simulate arrival times of radio emissions to 1 au for several sets of parameters assuming a presence of both the fundamental and harmonic components. Contrary to Thejappa et al. (2007), we have used a larger number of rays (100,000 rays instead of 1000 rays), a finer simulation grid ($\Delta S = l$ versus $\Delta S = 10l$), and variable values of the inner scale l_i. Specifically, we assumed a linear increase of l_i with distance R as $l_i = (R/R_{\mathrm{S}})$ km for $R < 100\,R_{\mathrm{S}}$, and $l_i = 100$ km for $R \geqslant 100\,R_{\mathrm{S}}$, where R_{S} represents the solar radius (Manoharan et al. 1987; Coles & Harmon 1989). Figure 5 shows histograms of simulated arrival times t_{MC} of rays generated at 375 kHz for four levels of the relative electron density fluctuations ($\epsilon = 0.05, 0.10, 0.15, 0.30$). We observe a similar exponential decay as for the *STEREO*/Waves measurements in Figure 2. We assume that the number of rays can be related to the flux density S. We have applied the same procedure as for *STEREO*/Waves data (Figure 2) to derive the decay times τ from these histograms. We calculated median values of the number of rays to estimate the background level. We analyze the shape of the histogram between the peak time (t_{peak}) and the last value above this level. We use Equation (1) to calculate the decay times τ. We have found that this model is in good agreement with the simulated data for the fundamental component. A comparison between observations (Figures 2(a) and (c)) and simulations of the fundamental component

4
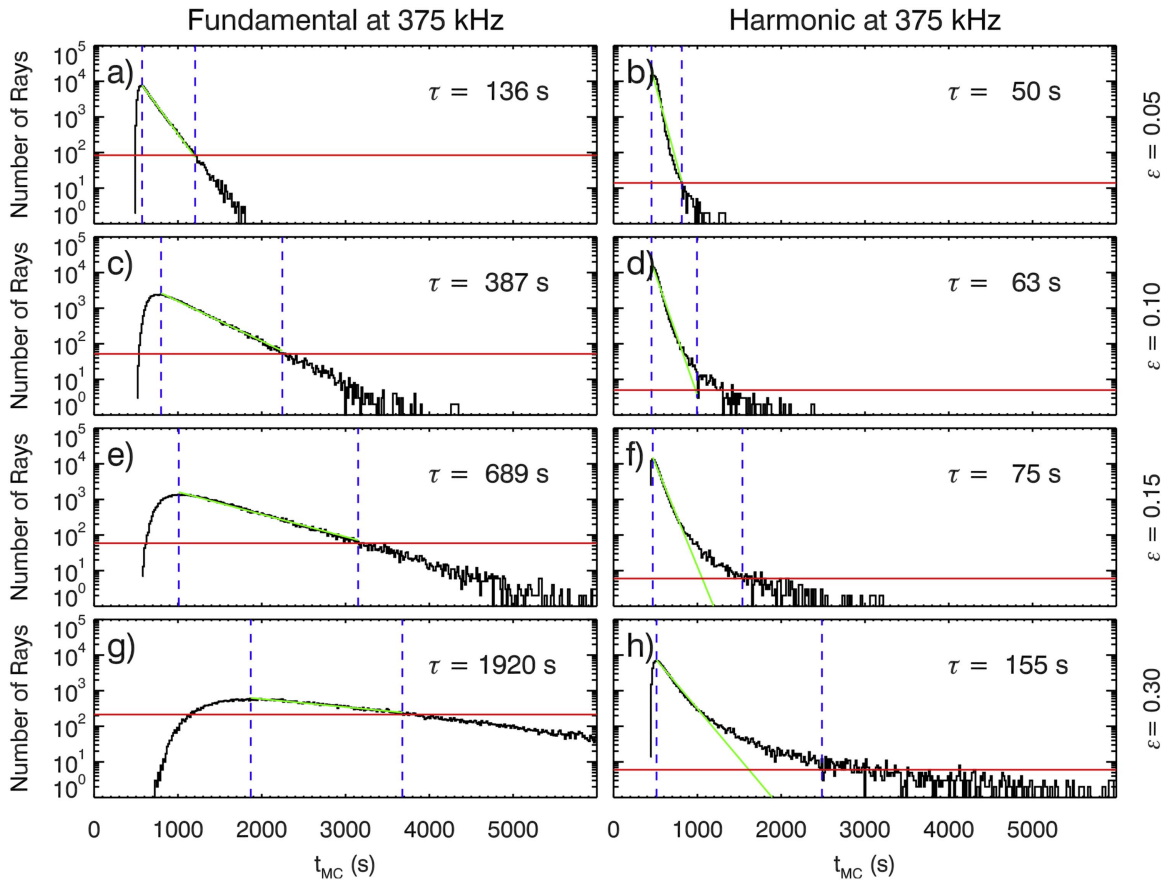
Figure 5. Results of Monte Carlo simulations at 375 kHz. (a)–(h) Histograms of simulated time arrivals t_{MC} of the fundamental (left) and harmonic emissions (right) at 375 kHz for various levels of relative electron density fluctuations ϵ. The red lines show the median values. The dashed lines denote the peak fluxes and last points above the median values. The green lines show the results of decay time fitting (Equation (1)).

(Figures 5(a) and (c)) suggests the relative electron density fluctuations ϵ to be between 0.05 and 0.10.

Although the exponential decay is also partly present for simulations of the harmonic component, we observe significant deviations from the exponential decay model for late phases of the arrival time. Moreover, simulated rise times are significantly shorter when compared to the observations. We performed Monte Carlo simulations for 17 frequency channels between 125 and 975 kHz corresponding to the *STEREO/Waves* measurements to reproduce radio flux density spectra (Figure 6). For each frequency channel, we calculated the simulated arrival time $t_{0.1c}$ assuming a constant beam speed of $0.1c$, which is typical for interplanetary type III radio bursts (Krupar et al. 2015):

$$t_{0.1c} = t_{MC} + \frac{r_i}{0.1c}, \qquad (4)$$

where r_i represents heliospheric distance from the model of Bougeret et al. (1984). While the simulated radio emission profiles of the fundamental component are consistent with the observations, results for the harmonic component are very narrow with short onset times. This indicates that this Monte Carlo simulation algorithm can be used to explain decay times of the fundamental component only.

We performed the Monte Carlo simulations for the same set of frequency channels and six levels of the relative electron density fluctuations ($\epsilon = 0.05, 0.06, 0.07, 0.08, 0.09, 0.10$) for the fundamental component only due to above-mentioned

discrepancies in the harmonic component. Figure 7 shows simulated and observed decay times τ versus f. We found that the simulated decay times τ have a power-law dependence on the frequency similar to those observed by *STEREO/Waves* (Figure 4). The simulated decay times increase with increasing the relative electron density fluctuations ϵ. We obtained comparable values of the simulated decay times τ with *STEREO* observations for relative electron density fluctuations $\epsilon = 0.06$–0.07.

3. Discussion and Summary

Although interplanetary type III bursts have been regularly measured for decades, we still do not have a proper model to explain their extremely large apparent source sizes, widespread visibility, nor to distinguish between fundamental and harmonic components. Recently, the *STEREO* spacecraft allow us to study type III bursts generated in the solar wind from two vantage points using identical radio instruments. We show an analysis of a type III burst that occurred on 2010 November 13 during the STEREO separation of 167° as an illustration of our analysis (Figure 1). We have found that the flux density S decreases exponentially over several decades at both spacecraft (Figure 2). We have investigated a large number of type III bursts in order to statistically retrieve their exponential decay times τ as a function of frequency f (Figure 3). Using a power-law model, we obtain a spectral index β of -1.18 ± 0.02 and -1.25 ± 0.02 for *STEREO-A* and *STEREO-B*, respectively
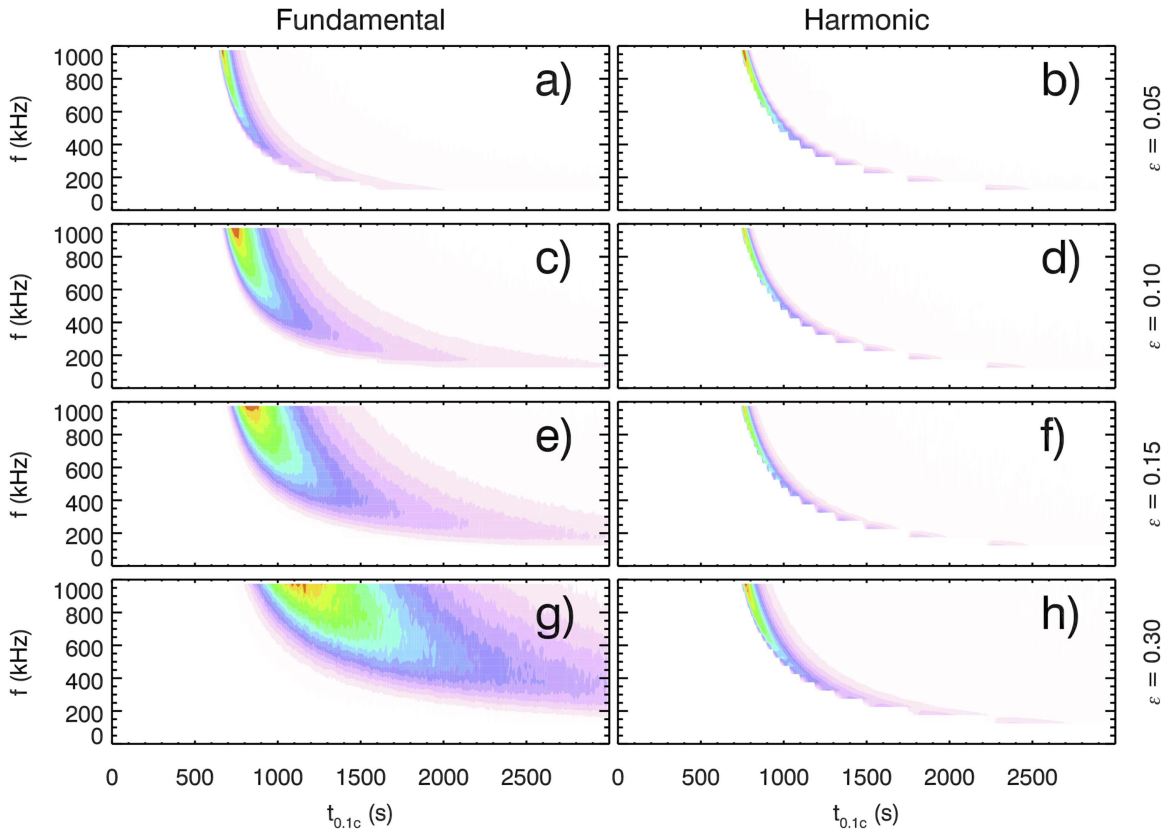
Figure 6. Results of Monte Carlo simulations between 125 and 975 kHz. (a)–(f) Radio flux density spectra of the fundamental (left) and harmonic emissions (right) for various levels of relative electron density fluctuations ϵ assuming an electron beam speed of 0.1c.
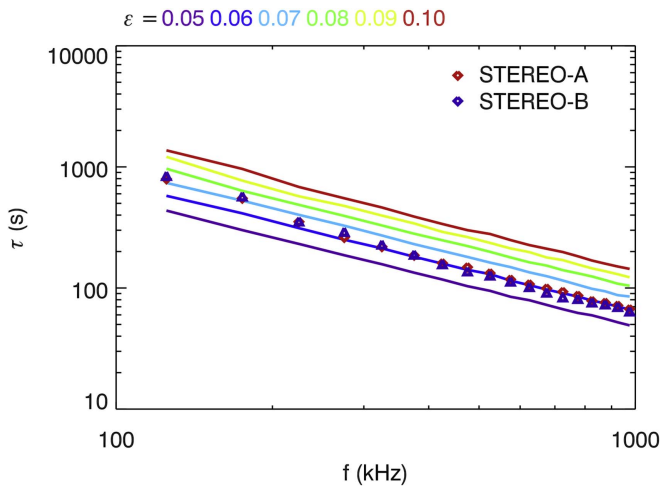
Figure 7. Results of Monte Carlo simulations between 125 and 975 kHz. Decay times as a function of frequency for the fundamental component. Red and blue diamonds show fitting results from *STEREO-A* and *STEREO-B*, respectively.

(Figure 4). The results obtained are comparable to those of previous studies.

We have implemented a Monte Carlo simulation technique to study the role of refraction and scattering for the fundamental and harmonic components separately. We note that following simplifications have been included in the Monte Carlo simulation code: (1) an isotropic point source, (2) a spherically symmetric solar wind electron density model, (3) a power-law distribution of the electron density fluctuations with spectral index agreeing with that of Kolmogorov, (4) an empirically derived model of the inner and outer scales of the electron density fluctuations, and (5) a constant value of the relative electron density fluctuations ϵ in the solar wind. These assumptions obviously affect our findings and can be improved in the future (e.g., a finite size dipole/quadrupole emission pattern, and a variable value of ϵ between the source and the observer). Nevertheless, the Monte Carlo simulations of the fundamental component perform very well in reproducing the *STEREO* observations (Figures 5 and 6). However, we observe deviations in the simulations of the harmonic component from measurements. Besides the above-listed simplifications, this can also indicate that we preferably observe only the fundamental component of interplanetary type III bursts, which is typically more intense. If one assumes that interplanetary type III bursts are emitted at the fundamental in reality, then our simplified scattering model explains the long tails on decay very well. If this assumption is not correct, and if most radio emissions are emitted at the harmonic, then our simplified model is missing some physics; e.g., it is possible that the source radio beam pattern is more dipolar or quadrupolar, instead of being isotropic (as we assumed in our simulations). Note, however, that until now, there have been no clear observational evidences to choose between fundamental or harmonic for interplanetary type III bursts.

From the arrival times, we calculated the decay times τ that we compare to those observed by *STEREO*/Waves (Figure 7). Our results suggest that the exponential decay of the observed flux density for the fundamental component can be explained by the scattering of radio signals by density inhomogeneities in the solar wind. The obtained relative electron density

fluctuations ϵ are 0.06–0.07 assuming the presence of the fundamental component. We note that this range depends on the initial assumptions of the inner and outer scales of the electron density fluctuations near actual radio sources. Nevertheless, our results will be soon challenged by in situ measurements of relative electron density fluctuations ϵ by the Solar Orbiter and Parker Solar Probe (Müller et al. 2013; Fox et al. 2016). Moreover, having a better understanding of the anisotropy of the density turbulence, which can affect radio-wave propagation from the type III source to the observer, is also important and will be the subject of future research.

ORCID iDs

V. Krupar ⓘ https://orcid.org/0000-0001-6185-3945
E. P. Kontar ⓘ https://orcid.org/0000-0002-8078-0902
O. Santolik ⓘ https://orcid.org/0000-0002-4891-9273
J. Soucek ⓘ https://orcid.org/0000-0003-0462-6804
J. P. Eastwood ⓘ https://orcid.org/0000-0003-4733-8319

References

Alvarez, H., & Haddock, F. T. 1973, SoPh, 30, 175
Bale, S. D., Ullrich, R., Goetz, K., et al. 2008, SSRv, 136, 529
Bastian, T. S. 1994, ApJ, 426, 774
Bastian, T. S. 1995, ApJ, 439, 494
Bastian, T. S., Benz, A. O., & Gary, D. E. 1998, ARA&A, 36, 131
Bavassano, B., & Bruno, R. 1995, JGR, 100, 9475
Bonnin, X., Hoang, S., & Maksimovic, M. 2008, A&A, 489, 419
Bougeret, J. L., Goetz, K., kaiser, M. L., et al. 2008, SSRv, 136, 487
Bougeret, J.-L., King, J. H., & Schwenn, R. 1984, SoPh, 90, 401
Cairns, I. H., & Robinson, P. A. 1995, ApJ, 453, 959
Coles, W. A., & Harmon, J. K. 1989, ApJ, 337, 1023
Dulk, G. A., Leblanc, Y., Robinson, P. A., Bougeret, J.-L., & Lin, R. P. 1998, JGR, 103, 17223
Dulk, G. A., & Suzuki, S. 1980, A&A, 88, 203
Ergun, R. E., Larson, D., Lin, R. P., et al. 1998, ApJ, 503, 435
Evans, L. G., Fainberg, J., & Stone, R. G. 1973, SoPh, 31, 501
Fox, N. J., Velli, M. C., Bale, S. D., et al. 2016, SSRv, 204, 7
Ginzburg, V. L., & Zhelezniakov, V. V. 1958, SvA, 2, 653
Gopalswamy, N., Aguilar-Rodriguez, E., Yashiro, S., et al. 2005, JGR, 110, A12S07
Haselgrove, J. 1963, JATP, 25, 397
Hollweg, J. V. 1968, AJ, 73, 972
Kellogg, P. J. 1980, ApJ, 236, 696
Kontar, E. P., Yu, S., Kuznetsov, A. A., et al. 2017, NatCo, 8, 1515
Krupar, V., Kontar, E. P., Soucek, J., et al. 2015, A&A, 580, A137
Krupar, V., Maksimovic, M., Santolik, O., Cecconi, B., & Kruparova, O. 2014a, SoPh, 289, 4633
Krupar, V., Maksimovic, M., Santolik, O., et al. 2014b, SoPh, 289, 3121
Krupar, V., Santolik, O., Cecconi, B., et al. 2012, JGR, 117, A06101
Leblanc, Y., Dulk, G. A., & Hoang, S. 1995, GeoRL, 22, 3429
Manoharan, P. K., Ananthakrishnan, S., & Pramesh Rao, A. 1987, in Proc. Sixth Int. Solar Wind Conf., ed. V. J. Pizzo, T. Holzer, & D. G. Sime (Boulder, CO: National Center for Atmospheric Research), 55
Martínez Oliveros, J. C., Lindsey, C., Bale, S. D., & Krucker, S. 2012, SoPh, 279, 153
Melrose, D. B. 1980, SSRv, 26, 3
Miteva, R., Samwel, S. W., & Krupar, V. 2017, JSWSC, 7, A37
Müller, D., Marsden, R. G., Cyr, O. C., St., & Gilbert, H. R. 2013, SoPh, 285, 25
Reiner, M. J., Goetz, K., Fainberg, J., et al. 2009, SoPh, 259, 255
Reiner, M. J., Kaiser, M. L., Fainberg, J., & Stone, R. G. 1998, JGR, 103, 29651
Steinberg, J. L., Hoang, S., & Dulk, G. A. 1985, A&A, 150, 205
Steinberg, J. L., Hoang, S., Lecacheux, A., Aubier, M. G., & Dulk, G. A. 1984, A&A, 140, 39
Stewart, R. T. 1974, SoPh, 39, 451
Thejappa, G., & MacDowall, R. J. 2008, ApJ, 676, 1338
Thejappa, G., MacDowall, R. J., & Kaiser, M. L. 2007, ApJ, 671, 894
Wild, J. P. 1950, AuSRA, 3, 541
Wohlmuth, R., Plettemeier, D., Edenhofer, P., et al. 2001, SSRv, 97, 9
Zaslavsky, A., Meyer-Vernet, N., Hoang, S., Maksimovic, M., & Bale, S. D. 2011, RaSc, 46, RS2008